Lab on a Chip

PAPER

View Article Online
View Journal | View Issue

CrossMark
click for updates

Cite this: *Lab Chip*, 2015, **15**, 2615

Sophisticated oil film geometries through incomplete electrical dewetting by feedback control and Fourier construction†

Wan-Lin Hsieh,[ab] Kuo-Ching Chen[b] and Jason Heikenfeld*[a]

Existing techniques for electronic control of the interface between two immiscible fluids are typically limited to simple periodic geometries (symmetric waves) or spherical geometries (only two principle radii of curvature). Presented here, is a new technique with much more sophisticated electronic control of fluid meniscus geometry. Previously undemonstrated two-fluid interfaces, such as asymmetric saw-tooth profiles, are created by dynamic modulation of an incomplete dewetting state for an oil film covering an array of control electrodes, with the oil film itself covered by an electrically conductive fluid acting as the ground electrode. Two distinct approaches are demonstrated: (1) application of voltages, electrical capacitance sensing of meniscus geometry, followed by further feedback control of the applied voltages based on the sensed electrical capacitance; (2) use of multiple periodic voltage waveforms and wave propagation across the meniscus to build up complex meniscus geometries by Fourier construction. These approaches are demonstrated in this work by a proven electro-hydrodynamic modeling method, which couples the Maxwell stress tensor with the laminar phase field of the oil–water dual phase. This work could serve numerous applications including particle or fluid transport (*e.g.* lab-on-chip), or adaptive optical surfaces (*e.g.* liquid prism arrays). Importantly, the results can be achieved using conventional materials, and the fluids respond with speeds that are adequately slow (ms–μs) such that even conventional control electronics (μs–ns) are more than adequate. Furthermore, because the conducting fluid never dewets the oil film from the solid surface, dielectric degradation issues are likely eliminated.

Reprinted from Lab on a Chip

Received 9th March 2015,
Accepted 7th May 2015

DOI: 10.1039/c5lc00274e

www.rsc.org/loc

Published on 07 May 2015. Downloaded by UNIVERSITY OF CINCINNATI on 01/06/2015 13:28:03.

Introduction

Electronic control of the geometry or transport of a fluid meniscus using dielectrophoresis[1] or electrowetting[2] is now a fairly mature field, even resulting in commercial products ranging from liquid lenses (Varioptic) to lab-on-chip devices (Illumina/Advanced Liquid Logic). The functional demonstrations are numerous and diverse, including droplet transport and mixing,[3,4] tunable lenses,[5,6] tiltable prism arrays,[7,8] displays,[9,10] diffraction gratings,[11] and pixel-free optical shutters.[12,13] However, these applications generally have several fundamental restrictions in common: (1) many, in practice, are limited to a spherical meniscus geometry (two principle radii of curvature[2]); (2) some are non-spherical, but provide only periodic and symmetric features;[11,14] (3) most are restricted to equilibrium profiles where the insulating fluid (typically an oil) is dewetted from a least a portion of an electrically charged surface. As a result, more sophisticated meniscus geometries, such as approximated saw-tooth or other complex meniscus profiles, have not been demonstrated. These types of fluid profiles could open up new opportunities in optics, such as phased arrays for beam steering,[15] periodic structures for diffraction gratings,[11] and could enable new forms of particle or fluid transport for lab-on-a-chip applications.[16]

Reported here is a new technique for much more sophisticated control of the geometry of a fluid meniscus. Previously undemonstrated geometries for two-fluid interfaces, such as asymmetric saw-tooth profiles, are created by dynamic modulation of an incomplete dewetting state for an oil film covering an array of control electrodes, with the oil itself covered by an electrically conductive fluid (see Fig. 1). Two electrodynamic methods are explored: (1) application of voltages, electrical capacitance based sensing of meniscus geometry, followed by further feedback control of the applied voltages based on electrical capacitance (see Fig. 1a); (2) use of multiple periodic voltage waveforms and wave propagation across the meniscus to build up complex meniscus geometries by Fourier construction (see Fig. 1b). Both of these techniques enable partial wetting of the oil film well past the conventional

[a] *Novel Devices Laboratory, Department of Electrical Engineering and Computing Systems, University of Cincinnati, Cincinnati, OH, 45230, USA.*
E-mail: heikenjc@ucmail.uc.edu
[b] *Institute of Applied Mechanics, National Taiwan University, Taipei, 10617, Taiwan*
† Electronic supplementary information (ESI) available: Supporting results. See DOI: 10.1039/c5lc00274e

Published on 07 May 2015. Downloaded by UNIVERSITY OF CINCINNATI on 01/06/2015 13:28:03.

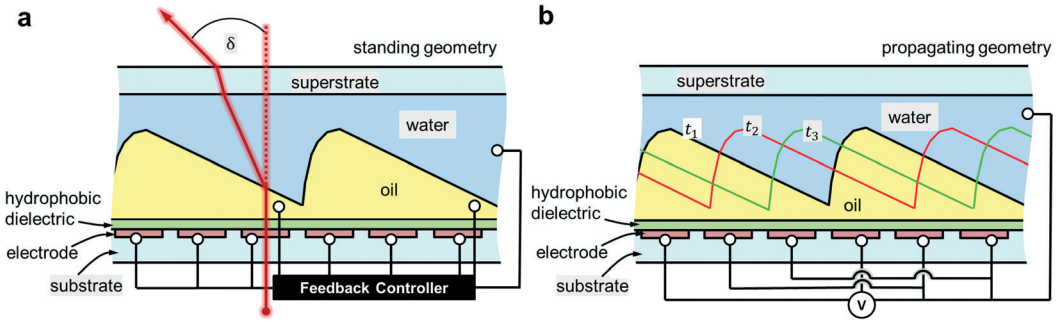


Fig. 1 Schematic illustration of device structure and operation. (a) Using feedback method to build up a saw-tooth profile, for example use as a Fresnel lens or phased array (see red arrow optical ray trace where δ is the steering angle). (b) Using multiple periodic voltage waveforms and wave propagation across the oil meniscus to build up complex meniscus geometries by Fourier construction. Here $t_1 < t_2 < t_3$. The feedback method of (a) will create geometries that appear static (although feedback control is inherently dynamic), and the wave method (b) will create geometries that will move horizontally with time.

point of instability for complete oil film breakup.[17] This is further practically important, because dielectric degradation issues common to electrowetting[18] are likely eliminated since the conducting fluid never completely breaks through the oil film. Several demonstrations are provided by numerical modeling, in which the electro-hydrodynamic (EHD) force deduced from the Maxwell stress tensor is coupled with the laminar phase field of the oil–water dual phase.[19] These modeling techniques are well-proven to track with experimental results, as demonstrated by our group previously for electrowetting-based displays[19,20] and dielectrowetting optical shutters.[21] Importantly, the results can be achieved using conventional materials, and the fluids respond with speeds that are adequately slow (ms–μs) such that even conventional control electronics (μs–ns) are more than adequate for potential applications.

Fundamentals and methods

Basic device structure and operation

As shown in Fig. 1, two approaches were explored. Both approaches utilize a bottom substrate which supports an array of patterned electrodes covered by a hydrophobic dielectric. The devices utilize a conducting fluid and an insulating fluid, for which there are numerous options,[22] but for which herein we will simply consider them to be an electrically conductive water phase and insulating dodecane oil phase. Unlike conventional electrowetting, the hydrophobic dielectric does not need to sustain the full applied voltage, because with this new approach, the conducting fluid is never allowed to fully wet through the oil film (any oil film always remains, the oil always wets the dielectric surface). Therefore the only requirement for the hydrophobic dielectric is that has an interfacial tension with the oil that is low enough to promote a Young's angle θ_Y of 180° (a complete oil film).[23] In this work, a uniformly flat oil height ranging from 5–18 μm is assumed to be the starting position for all experiments. Uniform oil film height could be achieved by the electronic control methods that will be taught herein, or by use of an array of widely-spaced hydrophobic pillars which could help pin the oil height (not shown). It is also interesting to note, that many of the aging issues which plague conventional electrowetting (dielectric degradation)[18] may not be an issue for the devices reported here as the water never comes in contact with the solid dielectric. Rather, the dielectric is mainly the oil, which is a fluid and inherently self-healing in terms of electrical defects. The full set of parameters for all materials relevant to the modeling results can be found in Table 1.

The device of Fig. 1a uses the feedback control method, referred to herein as the 'feedback method'. The feedback method uses application of voltages even possibly beyond the point of stability for a complete oil film, electrical capacitance based sensing of meniscus geometry, followed by further feedback control of the applied voltages based on electrical capacitance to maintain an oil film geometry where the water never reaches the hydrophobic dielectric surface. The example in Fig. 1a, is that of an saw-tooth profile but almost any combination of vertically oriented convex and concave oil geometries are likely possible if adequate electrodes and controls are implemented, and if the aspect ratio is not too great.

The device of Fig. 1b creates propagating waves in the oil and in some cases superposition of multiple created waves of different frequencies (Fourier construction), referred to herein as the 'wave method'. The 'wave method' requires multiple periodic voltage waveforms to generate the wave frequencies that comprise the geometries resulting from superposition.

Table 1 Material and interfacial properties used for simulations

Parameters	Quantity	Symbol	Value
Material properties	Density of oil	ρ_{oil}	884 kg m^{-3}
	Density of water	ρ_{water}	999.62 kg m^{-3}
	Viscosity of oil	μ_{oil}	2 cP
	Viscosity of water	μ_{water}	1.0093 cP
	Dielectric constant of oil	ε_{oil}	2.2
	Dielectric constant of water	ε_{water}	80
	Dielectric constant of hydrophobic dielectric layer	ε_{hyd}	3
Interfacial properties	Surface tension of oil and water	γ_{ow}	40 mN m^{-1}
	Contact angle of hydrophobic surface	θ_{hyd}	160°

Reprinted from Lab on a Chip

This journal is © The Royal Society of Chemistry 2015

Published on 07 May 2015. Downloaded by UNIVERSITY OF CINCINNATI on 01/06/2015 13:28:03.

Before delving into the specific results of this work, several additional points should be briefly discussed. Both the feedback method and wave method will be discussed in detail. Of course, these two methods could also be combined (wave propagation, Fourier construction, and feedback control), but such combination is not reported in this work. It is important to note, that the feedback method shown in Fig. 1a will create geometries that appear static (although feedback control is inherently dynamic), and the wave method will create geometries that will move horizontally with time. Lastly, because the demonstrations in this paper are created by modeling, a comparison to complex experimental dewetting behavior in electrowetting pixels[17,24,25] is provided with the online ESI† for this paper, to increase confidence in the predictions provided by the model. The same modeling performed in this work has also been published by our group for dielectrowetting and electrowetting devices, and also shown to closely track experimental results.[19–21]

Exploring the limit of oil film stability against dewetting

The modeling results begin with exploration of the limit of oil film stability against dewetting. These results reveal the requirement for feedback control if significant slopes or curvatures are to be implemented onto the meniscus of the oil film. As shown in Fig. 2a, the setup includes a 5 μm oil film covering a 1 μm hydrophobic dielectric layer with electrode width w_e = 25 μm and gap width between electrodes of w_g = 25 μm.

First, the time evolution of the dewetting process for the oil under an abruptly applied 20 V is shown in Fig. 2a, from which the water phase fully wets through the oil phase at t = 114 μs. Unlike the instabilities for complete oil film breakup with a large planar electrode (again, see online ESI† and previous work[17]), the patterned electrodes themselves determine the periodic dewetting profile for the oil. Fig. 2b provides the corresponding electric field strength calculated at the surface of the dielectric layer from x = 0 to 100 μm during the dewetting process from t = 0 to 114 μs. At the position where the water has wetted through the oil to the hydrophobic surface, the difference of electric potential across the hydrophobic dielectric layer is approximately equal to the external applied voltage. The plot also properly reveals high-field points (spikes) due to the sharp electrode edges. Fig. 2c shows the equivalent capacitance per unit area $C_{eq.}(t)$ (connected in series by oil film and hydrophobic dielectric layer) and the local oil height $h_{oil}(t)$ as function of time. The calculation for $C_{eq.}$ is presented in the Appendix section. Apparently, $C_{eq.}(t)$ increases as $h_{oil}(t)$ decreases. In addition, it could be found that when the oil film is dewetted, $C_{eq.} = C_{hyd}$. Next, as shown in Fig. 2d, the fluid dewetting speed is parametrically analyzed. As shown in Fig 2d, the time requirement is measured for the oil surface to reach the wave amplitude A = 1 μm with different applied voltages for a 5 μm oil film (see Fig. 2a for a labeling of A). These results confirm that switching speeds of fluids are adequately slow (ms–μs) such that even conventional control electronics (μs–ns) will be more than adequate for feedback control. Easily, even more viscous oils could be utilized to slow the dewetting speeds and to more rapidly dampen disturbances on the oil meniscus. Lastly, as shown in Fig. 2e, the equilibrium amplitude A and local oil height h_{oil} are recorded as voltage is slowly increased from 0 to 11 V (allowing equilibrium before each voltage step). The data shows that stable sinusoidal profiles can be generated for only A from 0 to 1.7 μm with corresponding for h_{oil} from only 5 to 4.15 μm. When the applied voltage is beyond ~11 V, the electrostatically induced oil film breakup occurs (limit of stability), thus leading to a periodic breakup into the space between the patterned electrodes. The fact that only a small change can be achieved for oil film thickness (4.15–5 μm) confirms our hypothesis that feedback control is mandatory if greater changes in oil film height are to be maintained.

Fundamentals of the feedback method

Fig. 3 shows the results of a simple control decision to avoid complete dewetting of the oil film, where the parameters used are identical to those of Fig. 2a. A control decision is created when the oil film reaches a thickness of $h_{oil}(t)$ = 0.5 μm, which is well beyond the point of stability previously illustrated in Fig. 2e. Such control decision could be easily sensed by measurement of electrical capacitance between the water and the electrode. No decision occurs infinitely quick, so in this experiment, an 'electronics control' delay time Δt_{delay} of 10 ns is inserted into the simulation before the voltage is decreased to 5 V to prevent complete oil dewetting. As shown in the Fig. 3, the oil film fully recovers at t = 400 μs. It should be noted that voltages that resulted in stable oil films such as 10 V shown previously in Fig. 2d, cannot be used at the $h_{oil}(t)$ = 0.5 μm decision point, because the oil is already much thinner than minimum stable thickness of the h_{oil} ~ 4 μm also shown in Fig. 2e. Fig. 3 gives a simple example of a single control-decision, and in the next section the continuous feedback method (looping) technique will be presented.

Results and discussion

Sophisticated oil film geometries created by the feedback method

In this section, first shown is continuous feedback control with a simple single electrode. Then, in the latter portion of this section, multi-electrode control and a sophisticated oil geometry is demonstrated. A basic decision loop is shown in Fig. 4a, and applies to a single electrode, meaning that if there were multiple electrodes each would have its own independent decision loop as well. First, a relatively high voltage V_1 (beyond point of oil film stability) is applied until the oil thickness $h_{oil}(t)$ (measured in the model as electric field magnitude) reaches the final expected value h_f (or E_f). Next the applied voltage is switched to V_2, which is safely before the point of stability for that reduced oil film height h_f. Then, as $h_{oil}(t)$ becomes larger than h_f the applied voltage is switched back to V_1 again, increasing the

Reprinted from Lab on a Chip

Published on 07 May 2015. Downloaded by UNIVERSITY OF CINCINNATI on 01/06/2015 13:28:03.

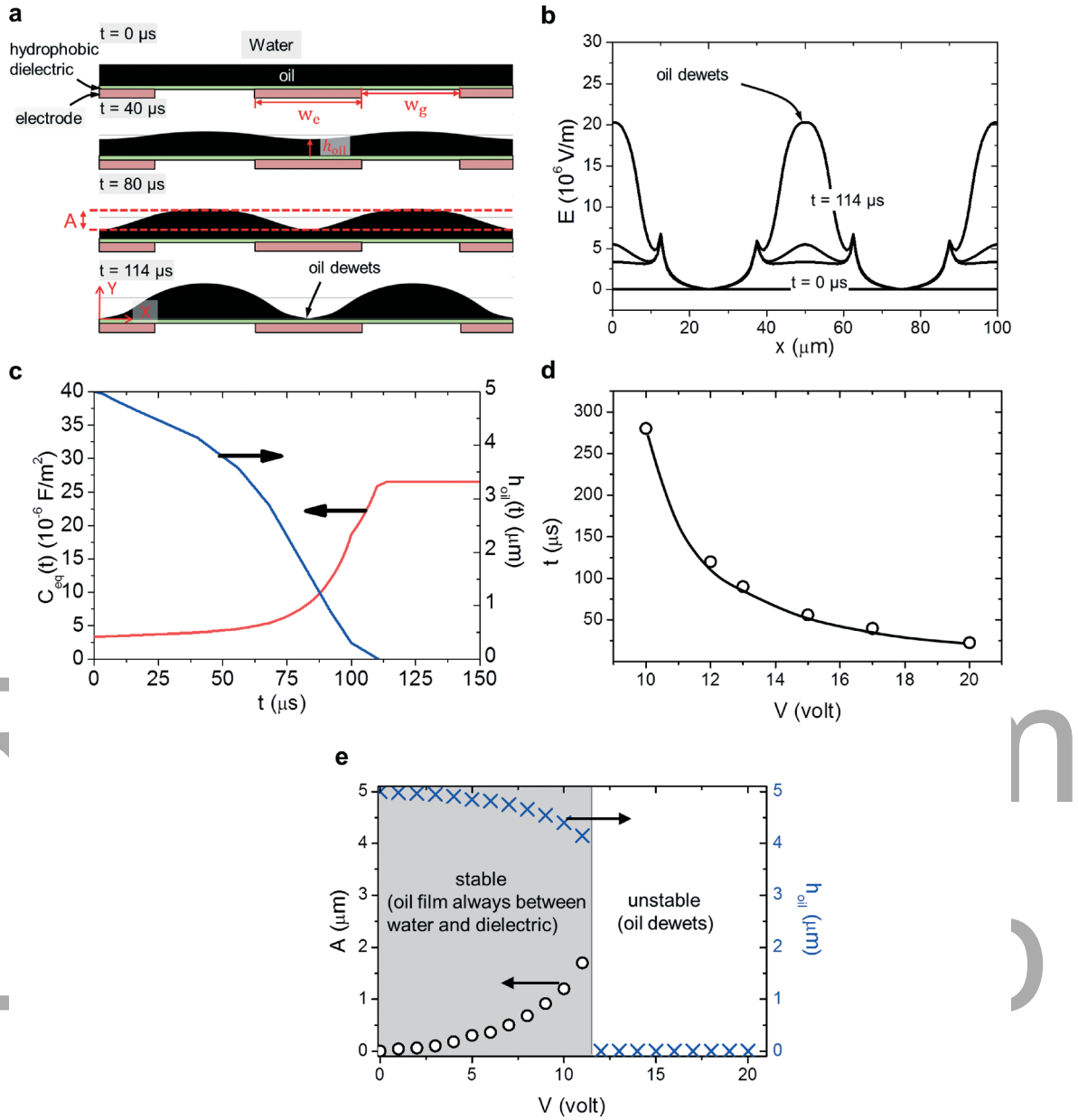


Fig. 2 Exploration of both partial and complete dewetting of patterned electrodes. (a) Time evolution of the oil film dewetting process with 20 V applied at t = 0 μs. Here A denotes the amplitude of the wave profile, and h_{oil} is the oil film height directly above the center of electrode. (b) Electric field calculated at dielectric layer surface during the dewetting process corresponding to the evolving states shown in (a). (c) Capacitance per unit area $C_{eq.}$ and h_{oil} as function of time. (d) The time requirement for the periodic wave profile taken to reach A = 1 μm with different applied voltages. (e) Plot of the equilibrium amplitude A and oil film h_{oil} *vs.* applied voltage. When the applied voltage is beyond ~11 V, the oil film is unstable and the water reaches the dielectric surface.

electromechanical pressure and the oil phase once again reverses in direction. Consequently, throughout the looping feedback method, the oil phase oscillates itself around the targeted height h_f. The amplitude of oscillation can be quite small if the delay time for decisioning is small and the fluid exhibits viscous damping.

A specific example for the decision loop of Fig. 4a is demonstrated in Fig. 4b for the case of h_f = 2.187 μm, which is well below the point of stability (h_{oil} ~ 4 μm) demonstrated in Fig. 2. The other parameters used in this example are the same as those in Fig. 2a, and the decision delay time is 10 ns. First applied is a relatively high voltage V_1 = 20 V, in which the oil will be dewetted by water without feedback control. When the local oil height is smaller than the designated value (h_f = 2.187 μm) the applied voltage is switched to V_2 = 5 V. Once $h_{oil}(t)$ is larger than h_f, the input voltage is then switched back to V_1 = 20 V, and so on… In total, with this version of feedback control, it only required ~80 μs to achieve the final oil film height. Furthermore, as shown in the inset diagram of Fig. 4b, the oscillation amplitude around h_f is only on the order of several nm, which interestingly for many optical applications is very far sub-wavelength (would not

 This journal is © The Royal Society of Chemistry 2015

Published on 07 May 2015. Downloaded by UNIVERSITY OF CINCINNATI on 01/06/2015 13:28:03.

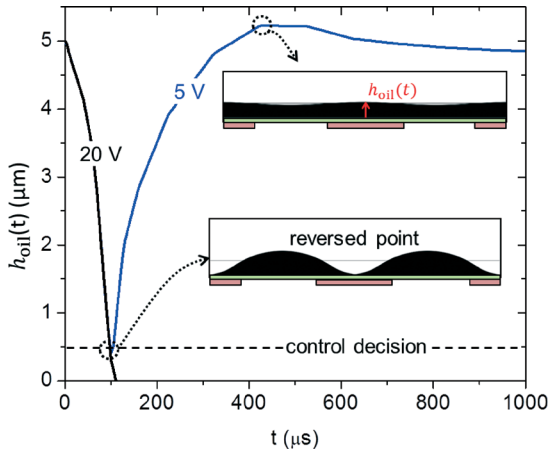


Fig. 3 An example of decision control. Plot of the time evolution of the oil film thickness with the control decision at an oil height of 0.5 μm to reduce the applied voltage from 20 V to 5 V. A 10 ns delay in implementation of the decision is included to mimic the delay associated with feedback control electronics which would sense oil film height through electrical capacitance between the water and electrode.

diffract or refract light propagation). This feedback control process would implement continuously to maintain $h_{oil}(t)$ at the designated point h_f as shown in the inset of Fig. 4b, or alternately, a new h_f setpoint could be set and similarly

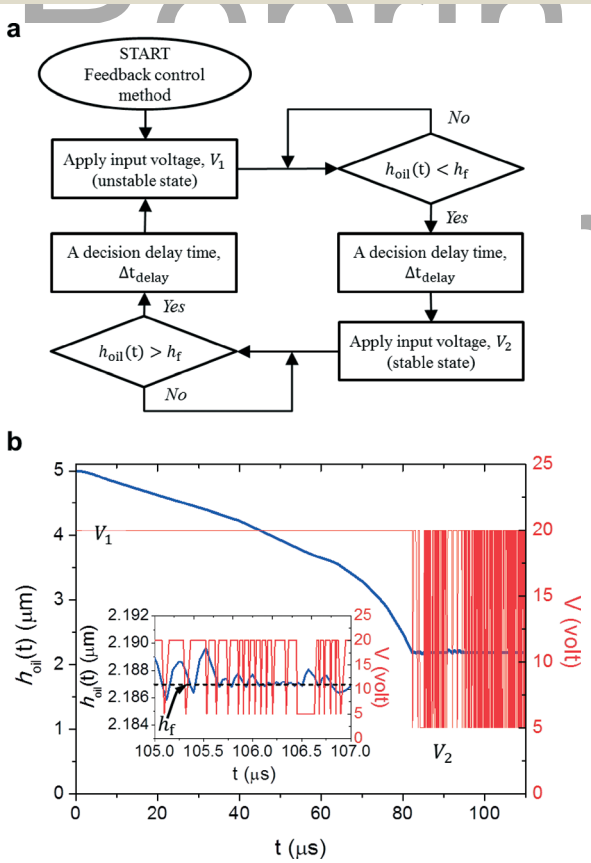


Fig. 4 Introduction of feedback control method. (a) Flow chart (decision loop) of the feedback method. (b) Plot of the oil film thickness $h_{oil}(t)$ as a function of time with feedback method. The inset shows the very small oscillation of the oil film height around the targeted thickness for 105 μs < t < 107 μs.

maintained. It should be noted, regarding potential electrical degradation due to leakage charge, that although a thick oil film still exists with a very low electric field (<10 V μm^{-1}), in practice, the voltage would likely be bipolar (alternating in polarity) to eliminate any net charge migration and electrode degradation. This is a practical issue, which does not effect the modeling results of this work other than electrical rise or fall times which are dependent on the output impedance of the electronic controls.

Next, multi-electrode control is demonstrated in order to build up more sophisticated asymmetric profiles. In this example, each electrode has its own voltage source and feedback control, and each is given its own target for the localized oil film height. Again, electrical capacitance could be the technique used to quickly predict the oil film height at any time. It was found, that reducing the width of electrode and/or increasing the oil film thickness was required to generate significantly asymmetric oil geometries. Therefore the demonstrated example utilizes a 10 μm oil film on patterned electrodes with w_e = w_g = 10 μm. The control decision delay time was again 10 ns. As seen in Fig. 5a, the simulation results show that asymmetric triangular profiles can be created in only t = 290 μs after starting from an initially flat oil film (t = 0 μs).

In this example, one triangular profile of width w is controlled by 5 electrodes, where the feedback method is implemented with (V_1, V_2) = (70 V, 5 V) at the first, fourth and fifth electrodes, and the second and third electrodes are switched off. An online video of this example is provided as Video S1.† The feedback control response of oil film thicknesses over each of the three actuated electrodes is plotted as a function of time as shown in Fig. 5b (again, corresponding to the time-lapse photographs in Fig. 5a). Not surprisingly, the electrode which requires the longest time to stabilize (the full 290 μs) involves the thinnest oil film height. A longer settling time is because: (1) the thinner the final oil film height the larger the change from the initial oil film height; and (2) the thinner the final oil layer the more difficult it is to control (less stable, stronger electric fields and meniscus velocities).

As an additional demonstration, asymmetric profiles were investigated with a smaller gap width between the electrodes (Fig. 5c, d). Here the array of patterned electrodes of w_e = 25 μm and w_g = 2 μm, were used with feedback controls of: Fig. 5c (V_1, V_2) = (70 V, 5 V) for d_{oil} = 10 μm, and; Fig. 5d (V_1, V_2) = (150 V, 10 V) for d_{oil} = 18 μm. For applications such as beam steering, the thicker the oil film the greater the steering angle δ that could be created. However, thicker oil films will require higher voltages for control. Of course, interfacial tension between the oil and water could be reduced, lowering the required voltage, but likely requiring longer times before the final oil geometry can be stabilized. Optimization of electrodes, voltages, fluids, interfacial tensions, and control methods, were not explored, and it is expected that much more triangular shapes for the fluids are certainly achievable. Regardless, the demonstration shown in Fig. 5 is unlike all previous forms of electrically controlled wetting/

Reprinted from Lab on a Chip

Published on 07 May 2015. Downloaded by UNIVERSITY OF CINCINNATI on 01/06/2015 13:28:03.

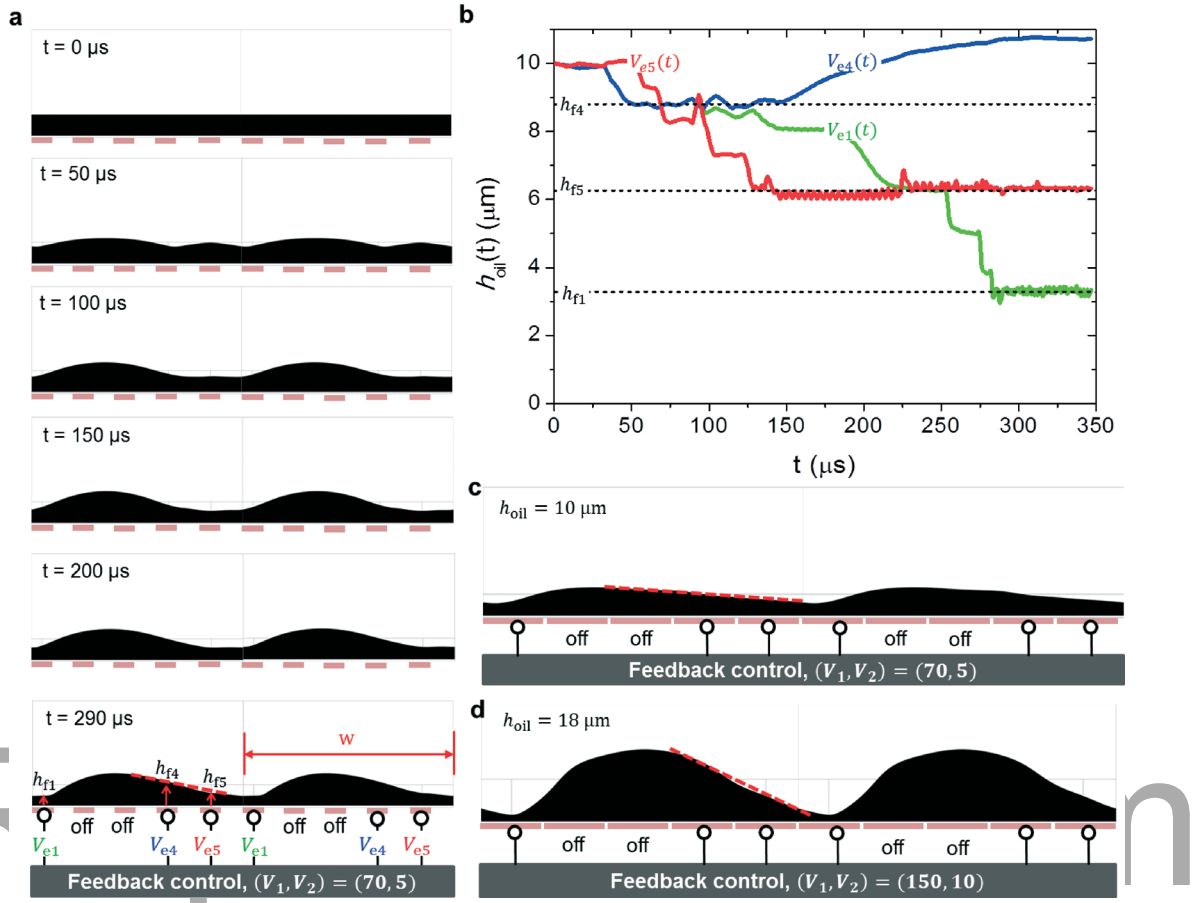


Fig. 5 Using the feedback method to build up triangular profiles. (a) An asymmetric triangular profile (t = 290 μs) is created from the initially flat oil film (t = 0 μs) based on the feedback method. (b) The plot of the oil film thickness $h_{oil}(t)$ above each of the three actuated electrodes as a function of time. (c, d) Plots of the fluid film profile with h_{oil} = 10 and 18 μm and a reduced gap width between electrodes.

Lab on a Chip

dewetting, as these results show a continuous oil film which has highly asymmetric shapes.

The number of electrodes required to generate a single standing asymmetric profile and the corresponding values of the expected oil height h_f above each electrode can be determined by a Fourier series approximation. This series has also been used to represent the complex interfacial profile of a rising liquid column under an external electric field.[26] Here, we consider a periodic function $h(x)$ of period w, and there are $N + 1$ equal-interval nodes between $x = 0$ and $x = w$. This corresponds to the proposed device that has $N + 1$ electrodes within the length of a segment, w. Thus, the oil height $h(x)$ in a Fourier series approximation based on initial oil thickness h_{oil} can be expressed as

$$h(x) = h_{oil}\left[1 + \sum_{n=1}^{N} A_n^N \sin\left(\frac{2N\pi x}{nw}\right)\right]. \quad (1)$$

This equation tells us that (i) the oil height $h(x)$ is related to the coefficients A_n^N, and (ii) an arbitrary wave-like function could not be attainable unless it obeys eqn (1). The detail of the Fourier series approximation is shown in the Appendix section. With N = 10, w = 100 μm, and h_{oil} = 10 μm, Fig. 6a

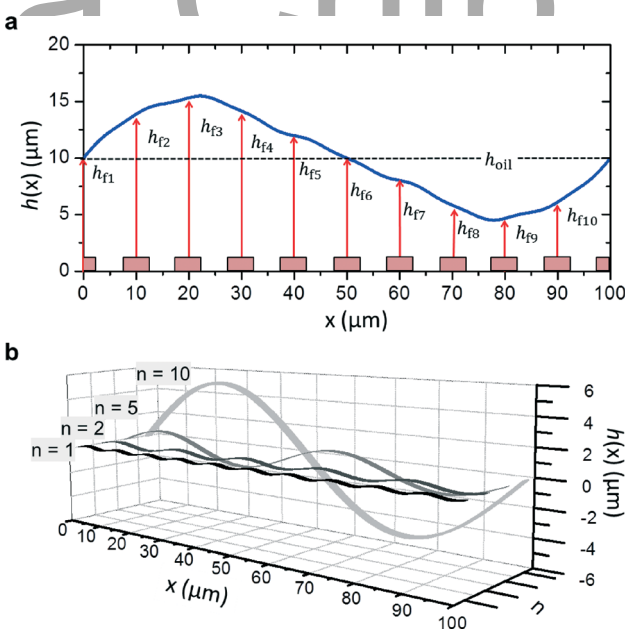


Fig. 6 Fourier approximation. (a) The approximately saw-tooth profile $h(x)$ according to the Fourier series approximation. The expected value h_{fn} at each node (or electrode) could be accurately predicted. (b) Basis functions when n = 1, 2, 5, and 10.

This journal is © The Royal Society of Chemistry 2015

Published on 07 May 2015. Downloaded by UNIVERSITY OF CINCINNATI on 01/06/2015 13:28:03.

demonstrates an example of a saw-tooth wave (not with fluids), which is constructed in terms of the basis functions plotted in Fig. 6b, where $A_1^{10} = 0.1$, $A_2^{10} = 0.2$, $A_5^{10} = 1$, and $A_{10}^{10} = 5$ are adopted. As N increases, obviously, the fidelity of the saw-tooth geometry can be improved.

The wave method (Fourier construction)

In the wave method, multiple periodic undulations of the oil (waves) are created and super-imposed to Fourier construct complex shapes (Fig. 6). At first, one might think of using the techniques of the feedback method as-is for Fourier construction of oil geometries, but then will realize, that creating multiple 'static waves' on an oil film is not possible. Rather, the waves must be propagating. This complicates the overall control, but might provide even finer control over the oil film geometry (steeper slopes, sharper corners). For example, because electric field is divergent, a perfectly sharp corner geometry in the oil film is physically impossible with the electrode format used. However, with Fourier construction, sharp corners are possible if enough waves are super-imposed. Propagating waves require low-viscosity fluids, such that viscous damping does not quickly diminish the wave. To help overcome viscous damping, it will be seen later in this section that the propagating waves will be reinforced by use of multiple electrodes.

Implementing a true Fourier construction with multi-electrode control was found to be beyond the present capability of the simulation capability used in this initial work. However, a simpler version of the wave method was demonstrated. Fig. 7a shows the steps in a process of using this simpler

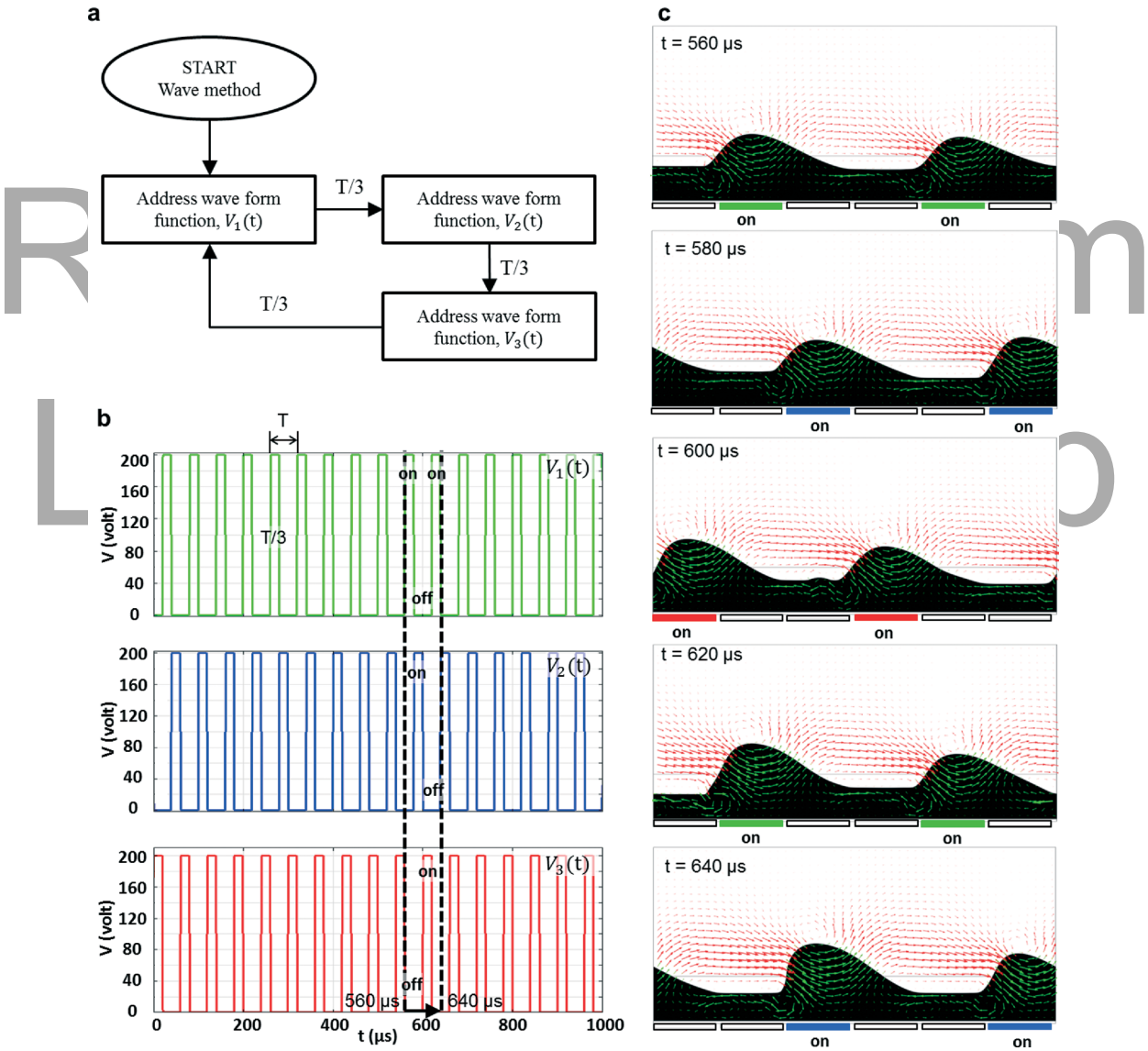


Fig. 7 Using a simplified wave method to build up triangular structures. (a) Flow chart for the simplified wave method where T is the period for one complete cycling of the three voltages. (b) Three different driving waveforms $V_1(t)$, $V_2(t)$, and $V_3(t)$ with $T/3$ duty cycle addressed across the fluids. (c) Simulated wave propagation using wave method from t = 560 to t = 640 μs, where triangular profiles are created. The green and red arrows denote the velocity field of oil and water, respectively. Colors for voltages in (b) correspond with electrode positions and colors shown in (c).

Published on 07 May 2015. Downloaded by UNIVERSITY OF CINCINNATI on 01/06/2015 13:28:03.

wave method for generating wave propagation and creating complex geometries such as a saw-tooth profile. Three driving waveforms $V_1(t)$, $V_2(t)$, and $V_3(t)$ with $T/3$ duty cycle are controlled to oscillate the fluids and to create or support fluid flow, where T is the time of a complete cycle as shown in Fig 7b. The fact that the fluid is *flowing* is further interesting, supporting speculation that this work could also be useful for lab-on-chip type applications where fluid flow is required. The parameters used for Fig. 7 are the same as those in Fig. 5d, and the amplitude and the time per complete cycle of the waveforms function is 200 V and 60 μs, respectively. Fig. 7c shows the simulation result of wave propagation from t = 560 to t = 640 μs, where triangular profiles are created. It should be noted that the duty cycle of the waveforms should be designed carefully. At t = 560 μs, for example, the waveforms of $V_1(t)$ is switched on in order to drive the wave to propagate to next electrode. After 20 μs ($T/3$), when the wave arrives at the next electrode $V_2(t)$ is switched on and $V_1(t)$ is switched off. As a result, the continuous wave propagation with triangular shape could be generated as seen in simulated results of Fig. 7c (a video is available as Video S2†). The results of Fig. 7c are for the example time period of operation bounded by the dotted lines in Fig. 7b. The velocity field of oil (green arrows) and water (red arrows) is also plotted in Fig. 7c. It is seen that the water phase near the triangular oil waves flows along the direction of wave propagation. This demonstration assumed an infinite region of water above the oil, and obviously the flow patterns would be effected if a finite channel height existed (*e.g.* like that shown in Fig. 1).

Conclusions

A new technique for much more sophisticated control of the geometry of a fluid meniscus has been successfully presented. Although the results are not from physical experimentation, again the modeling techniques have been previously proven against experiment, and the time-scales needed for electronics control are adequately slow such that real-world implementation is expected to reproduce the results reported here. Again, the results are un-optimized, and additional geometries and finer control over geometry is expected with further work. Furthermore, the control algorithm utilized here is quite basic, and far more advanced algorithms are expected to result in both faster changes in oil shape (reduced settling time) and even greater geometry asymmetries. Furthermore, for applications where the ~100 μs switching speeds demonstrated herein are not needed, fluid interfacial surface tensions can be reduced to 0.1's to 1's of mN m^{-1} and voltages reduced to the point where even thicker oil films could be used for steeper oil geometries, and/or also allowing for much lower voltages. The electrode dimensions demonstrated in this work are 10 μm or greater, such that analog Silicon feedback control circuitry could be implementable even with two-dimensional electrode arrays and fluid control.[27] Furthermore, in some applications, simple one-dimensional asymmetry is adequate, and long column electrodes could be used along with external control circuitry. Other interesting possibilities include reflective fluid interfaces, enabled by Janus particles[28] or thin flexible films.[29] The key outcome of this work, is to stimulate different thought of wetting control compared to how it has been dominantly performed in the past. In the past, outside of droplet oscillation experiments,[14] typically a fairly static stimulus is applied and a one or two fluid system allowed to reach equilibrium. This is even true for feedback control of electrowetting prisms,[30] where feedback control based on capacitance measurement is used, but the fluid system involves complete breakup of an oil film and an oil film geometry that has constant radius of curvature. In the work reported here, a wider array of geometries is possible. Furthermore, the net fluid flow for the wave method is interesting because the 'pumping mechanism' is localized, which can increase the velocity of fluid flow compared to techniques like electrowetting where the force is limited to the advancing edge of the fluid. In addition, this work opens up interesting opportunities in controlling a fluid meniscus irrespective of the influence of a triple point (contact line), as the water never touches the dielectric surface to form a triple point. Lastly, from an applied perspective, the fact that the conducting fluid never has to touch the electrode or dielectric, could result in extreme longevity for the devices.[18] A wide range of new theoretical and applied investigations are possible, with further development of the feedback and wave methods that have been reported here.

Reprinted from Lab on a Chip

Appendix

Calculation for the equivalent capacitance

The equivalent capacitance, $C_{eq.}(t)$, connected by the two capacitors, oil film ($C_{oil} = \varepsilon_0\varepsilon_{oil}/h_{oil}(t)$) and hydrophobic dielectric layer ($C_{hyd} = \varepsilon_0\varepsilon_{hyd}/h_{hvd}$), can be expressed by

$$C_{eq.}(t) = \frac{C_{oil}C_{hyd}}{C_{oil}+C_{hyd}} = \frac{\varepsilon_0\varepsilon_{oil}\varepsilon_{hyd}}{h_{oil}(t)\varepsilon_{hyd}+h_{hyd}\varepsilon_{oil}}, \quad (2)$$

where h_{oil}(t) is the oil film height measured directly above the center of the electrode, ε_0 is the permittivity of vacuum, and the values of ε_{oil} and ε_{hvd} are shown in Table 1.

Fourier series approximation

A wave-like function could be represented through eqn (1) if the coefficient A_n^N associated with each mode n is determined. It should be noted that n must be the divisor of N due to the assumption of the periodic condition, *i.e.*, $h(x) = h(x + w)$. Now we define a dimensionless function $\xi(x)$ as

$$\xi(x) = \left[h(x)/h_{oil}\right] - 1 = \sum_{n=1}^{N} A_n^N \sin\left(\frac{2N\pi x}{nw}\right). \quad (3)$$

The coefficient A_n^N could be obtained from multiplying eqn (3) by the functions $\sin(2N\pi x/mw)$, and then integrating the

 This journal is © The Royal Society of Chemistry 2015

Published on 07 May 2015. Downloaded by UNIVERSITY OF CINCINNATI on 01/06/2015 13:28:03.

resulting series from $x = 0$ and $x = w$. From the orthogonality condition, we are led to

$$A_n^N = \frac{2}{w}\int_{x=0}^{x=w} \xi(x)\sin\left(\frac{2N\pi x}{nw}\right)\mathrm{d}x, \quad (4)$$

which links the coefficient A_n^N and the local height of oil film $h(x)$.

Simulation of dynamic moving interface

We adopt the Phase Field Method (PFM) to solve the dynamic moving interface problem.[31] The moving interface between oil and water is set as a tiny nonzero-thickness transition region. Thus, the physical properties at the interface could be described by functions within this region with the use of a continuous phase-field variable ϕ, which varies from −1 for water to 1 for oil. From the introduced volumetric fractions $\bar{V}_{\mathrm{water}} = (1 - \phi)2$ and $\bar{V}_{\mathrm{oil}} = (1 + \phi)/2$, the physical quantities within the transition region are given as

$$\begin{aligned}\rho &= \rho_{\mathrm{water}}\bar{V}_{\mathrm{water}} + \rho_{\mathrm{oil}}\bar{V}_{\mathrm{oil}}\\ \mu &= \mu_{\mathrm{water}}\bar{V}_{\mathrm{water}} + \mu_{\mathrm{oil}}\bar{V}_{\mathrm{oil}}\\ \varepsilon &= \varepsilon_{\mathrm{water}}\bar{V}_{\mathrm{water}} + \varepsilon_{\mathrm{oil}}\bar{V}_{\mathrm{oil}},\end{aligned} \quad (5)$$

where ρ, μ, and ε represent the density, viscosity, and dielectric constant of fluids, respectively. In the diffusive-interface picture, the evolution of the interface between oil and water is governed by the Cahn–Hilliard convection equation[32]

$$\frac{\partial\phi}{\partial t} + \mathbf{u}\cdot\nabla\phi = \nabla\cdot(M\nabla G), \quad (6)$$

where $\mathbf{u}$ represents the fluid velocity, M denotes the mobility (or diffusion coefficient), and G is the chemical potential. The mobility can be expressed as $M = \chi h_{\mathrm{PF}}^2$, where χ is the characteristic mobility and h_{PF} is the capillary width that scales with the thickness of the diffuse interface in PFM. The chemical potential, which is a partial differential of the total free energy with respect to ϕ, could be expressed as $G = \eta[-\nabla^2\phi + \phi(\phi^2 - 1)/h_{\mathrm{PF}}^2]$, where η is the energy density parameter. In addition, η and h_{PF} are related to the oil–water interfacial tension through the relation: $\gamma_{\mathrm{ow}} = 2\sqrt{2}\lambda/3h_{\mathrm{PF}}$.

Simulation of electric field

The static electric field in the hydrophobic dielectric layer, oil phase, and water phase, is assumed to be governed by the Laplace equation

$$\nabla\cdot(\varepsilon_0\varepsilon_{\mathrm{r}}\nabla V) = 0, \quad (7)$$

where ε_0 is the vacuum permittivity, ε_{r} is the relative permittivity of the numerical domains including both solid dielectrics and fluids, and V is the electric potential. Here, it should be noted that the assumption of leaky dielectric (no electric charge density) in eqn (7) is adopted to help simplify the electrostatic equation of the water phase.[19]

Simulation of flow field

The transport of mass and momentum governed by the incompressible Navier–Stokes equations

$$\rho\left(\frac{\partial\mathbf{u}}{\partial t} + \mathbf{u}\cdot\nabla\mathbf{u}\right) = -\nabla p + \nabla\cdot\mu\left(\nabla\mathbf{u} + \nabla\mathbf{u}^T\right) + \mathbf{F}_{\mathrm{S}} + \mathbf{F}_{\mathrm{E}}, \quad (8a)$$

$$\nabla\cdot\mathbf{u} = 0, \quad (8b)$$

where ρ and μ are the density and viscosity of the fluids, which take the form as in eqn (5). p, $\mathbf{F}_{\mathrm{S}}$, $\mathbf{F}_{\mathrm{E}}$ respectively denote the pressure, the volumetric surface tension, and the volumetric electrodynamic force generated by an electric field. In the PFM, $\mathbf{F}_{\mathrm{S}}$ can be calculated over the computational domain in terms of the chemical potential and phase-field variable by

$$\mathbf{F}_{\mathrm{S}} = G\nabla\phi. \quad (9)$$

Obviously, $\mathbf{F}_{\mathrm{S}}$ approaches zero except those at the diffusive thickness of the oil–water interface. The volumetric electrodynamic force $\mathbf{F}_{\mathrm{E}}$, a net effect of an applied electric field acting on the fluids, can be expressed by the divergence of the Maxwell stress tensor $\mathbf{T}^{\mathbf{M}}$

$$\mathbf{F}_{\mathrm{E}} = \nabla\cdot\mathbf{T}^{\mathbf{M}}. \quad (10)$$

In component expression, T_{ij}^{M} is written as

$$T_{ij}^{\mathrm{M}} = \varepsilon E_i E_j - \frac{\varepsilon}{2}\delta_{ij}E_k E_k, \quad (11)$$

where δ_{ij} is the Kronecker delta function, and $i, j = x, y, z$.

Boundary conditions

In the formulation of PFM, the boundary condition for the hydrophobic surface is considered as a wetted wall, and along the surface we specify a wetted contact angle θ_{w}, which is related to ϕ through

$$\mathbf{n}\cdot\nabla\phi = \cos\theta_{\mathrm{w}}|\nabla\phi|, \quad (12)$$

where $\mathbf{n}$ is the unit vector normal to the wall.

The no-slip boundary condition (*i.e.*, $\mathbf{u} = 0$) is used to associate with the momentum eqn (8a) and (8b). Furthermore, the periodic condition is adopted at the two outlets of the simulated domain.

When solving the electrostatic field from the Laplace equation in eqn (7), the zero charge condition (*i.e.*, $\mathbf{n}\cdot\mathbf{D} = 0$) is adopted for the gaps between electrodes. In addition, the periodic condition that $V_{\mathrm{in}} = V_{\mathrm{out}}$ is adopted at the outlets of the simulated domain.

Reprinted from Lab on a Chip

Published on 07 May 2015. Downloaded by UNIVERSITY OF CINCINNATI on 01/06/2015 13:28:03.

Acknowledgements

This work is supported by the National Science Council, Taiwan, under the grant MOST 103-2221-E-002-070.

References

1 T. B. Jones, M. Gunji, M. Washizu and M. Feldman, *J. Appl. Phys.*, 2001, **89**, 1441–1448.
2 F. Mugele and J. Baret, *J. Phys.: Condens. Matter*, 2005, **17**, R705–R774.
3 P. Paik, V. K. Pamula, M. G. Pollack and R. B. Fair, *Lab Chip*, 2003, **3**, 28–33.
4 S. K. Cho, H. Moon and C. J. Kim, *J. Microelectromech. Syst.*, 2003, **12**, 70–80.
5 B. Berge and J. Peseux, *Eur. Phys. J. E*, 2000, **3**, 159–163.
6 S. Kuiper and B. H. W. Hendriks, *Appl. Phys. Lett.*, 2004, **85**, 1128–1130.
7 N. R. Smith, D. C. Abeysinghe, J. W. Haus and J. Heikenfeld, *Opt. Express*, 2006, **14**, 6557–6563.
8 L. Hou, J. Zhang, N. Smith, J. Yang and J. Heikenfeld, *J. Micromech. Microeng.*, 2010, **20**, 015044.
9 R. A. Hayes and B. Feenstra, *Nature*, 2003, **425**, 383–385.
10 K. Zhou, J. Heikenfeld, K. A. Dean, E. M. Howard and M. R. Johnson, *J. Micromech. Microeng.*, 2009, **19**, 065029.
11 C. V. Brown, G. G. Wells, M. I. Newton and G. McHale, *Nat. Photonics*, 2009, **3**, 403–405.
12 M. Hagedon, S. Yang, A. Russell and J. Heikenfeld, *Nat. Commun.*, 2012, **3**, 1173.
13 R. Zhao, B. Cumby, A. Russell and J. Heikenfeld, *Appl. Phys. Lett.*, 2013, **103**, 223510.
14 J. M. Oh, S. H. Ko and K. H. Kang, *Langmuir*, 2008, **24**, 8379–8386.
15 P. F. McManamon, P. J. Bos, M. J. Escuti, J. Heikenfeld, S. Serati, H. Xie and E. A. Watson, *Proc. IEEE*, 2009, **97**, 1078–1096.
16 J. Berthier, *Micro-drops and Digital Microfluidics*, William Andrew, Norwich, 2012.
17 B. Sun and J. Heikenfeld, *J. Micromech. Microeng.*, 2008, **18**, 025027.
18 A. Schultz, S. Chevalliot, S. Kuiper and J. Heikenfeld, *Thin Solid Films*, 2013, **534**, 348–355.
19 W. L. Hsieh, C. H. Lin, K. L. Lo, K. C. Lee, W. Y. Cheng and K. C. Chen, *J. Micromech. Microeng.*, 2014, **24**, 125024.
20 R. L. J. Chang, P. W. Liu, C. Y. Wu, P. P. Cheng, J. L. Chen, K. C. Chen and W. L. Hsieh, *SID Symp. Dig. Tech. Papers*, 2014, vol. 45, pp. 785–788.
21 A. Russell, W. L. Hsieh, K. C. Chen and J. Heikenfeld, *Langmuir*, 2015, **31**, 637–642.
22 S. Chevalliot, J. Heikenfeld, L. Clapp, A. Milarcik and S. Vilner, *J. Disp. Technol.*, 2011, **7**, 649–656.
23 M. Maillard, J. Legrand and B. Berge, *Langmuir*, 2009, **25**, 6162–6167.
24 S. Herminghaus, *Phys. Rev. Lett.*, 1999, **83**, 2359.
25 A. Staicu and F. Mugele, *Phys. Rev. Lett.*, 2006, **97**, 167801.
26 T. B. Jones, K. L. Wang and S. Bei, *13th Int'l Coating Science and Technology Symposium*, 2006.
27 H. Washio, K. Maeda, Y. Kaise, Y. Kubota, M. Hijikigawa, M. Brownlow and G. Cairns, *SID Symp. Dig. Tech. Papers*, 2001, vol. 32, pp. 276–279.
28 M. A. Bucaro, P. R. Kolodner, J. A. Taylor, A. Sidorenko, J. Aizenberg and T. N. Krupenkin, *Langmuir*, 2008, **25**, 3876–3879.
29 L. Hou, N. R. Smith and J. Heikenfeld, *Appl. Phys. Lett.*, 2007, **90**, 251114.
30 B. de Boer, F. Suijver, M. Megens, S. Deladi and S. Kuiper, *J. Appl. Phys.*, 2010, **107**, 063101.
31 P. Yue, J. J. Feng, C. Liu and J. Shen, *J. Fluid Mech.*, 2004, **515**, 293–317.
32 J. W. Cahn and J. E. Hilliard, *J. Chem. Phys.*, 1958, **28**, 258–267.

Reprinted from Lab on a Chip

This journal is © The Royal Society of Chemistry 2015